Effect of injection water ionic strength on estimating hydraulic parameters in a 3D sand tank using silica encapsulated magnetic DNA particles

Chakraborty, Swagatam; Elhaj, Rayan; Foppen, Jan Willem; Schijven, Jack

DOI
10.1016/j.advwatres.2023.104507

Publication date
2023

Document Version
Final published version

Published in
Advances in Water Resources

Citation (APA)
Chakraborty, S., Elhaj, R., Foppen, J. W., & Schijven, J. (2023). Effect of injection water ionic strength on estimating hydraulic parameters in a 3D sand tank using silica encapsulated magnetic DNA particles. *Advances in Water Resources*, *179*, Article 104507. https://doi.org/10.1016/j.advwatres.2023.104507

Advances in Water Resources 179 (2023) 104507

Contents lists available at ScienceDirect

Advances in Water Resources

journal homepage: www.elsevier.com/locate/advwatres

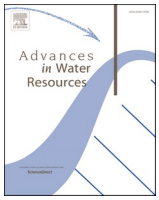

Effect of injection water ionic strength on estimating hydraulic parameters in a 3D sand tank using silica encapsulated magnetic DNA particles

Swagatam Chakraborty [a,*], Rayan Elhaj [b], Jan Willem Foppen [d], Jack Schijven [a,c]

[a] Environmental Hydrogeology Group, Department of Earth Sciences, Utrecht University, Princetonlaan 8a, Utrecht 3584 CB, the Netherlands
[b] Department of Water Sciences and Engineering, IHE-Delft, Institution for Water Education, Westvest 7, Delft 2611 AX, the Netherlands
[c] Department of Statistics, Informatics and Modelling, National Institute of Public Health and the Environment, P.O.Box 1, Bilthoven 3720 BA, the Netherlands
[d] Water Resources Section, Department of Civil Engineering and Geosciences, Delft University of Technology, Delft, the Netherlands

ARTICLE INFO

Keywords:
Colloids
Hydraulic conductivity
Effective porosity
Longitudinal dispersivity
Sand tank

ABSTRACT

We investigated the applicability of Silica encapsulated, superparamagnetic DNA particles (SiDNAmag) in determining aquifer hydraulic parameters at different ionic strengths (1 mM, 5 mM, and 20 mM phosphate buffer) of injection suspension. Thereto, in a homogeneous, unconsolidated sand tank we pulse - injected two uniquely sequenced SiDNAmag at two injection points. At 0.5 m and 0.8 m downstream from the injection points, we measured the concentration of SiDNAmags at three vertically distributed and two horizontally distributed sampling locations. We estimated the hydraulic parameter distributions from the SiDNAmag breakthrough curves through a Monte – Carlo approach and compared the parameter distributions with salt tracer breakthrough curves. Our results indicated that at all the ionic strengths, the times of peak concentrations, and the shapes of the breakthrough curves were similar to the salt tracer. As compared to the salt, a 1 – 3 log units reduction in the maximum effluent concentration of SiDNAmag was due to kinetic attachment. The attachment rate reduced from 1 mM to 5 mM phosphate buffer possibly due to competitive adsorption of phosphate onto the favourable attachment sites. SiDNAmag attachment rate further increased in 20 mM buffer suspension, possibly due to the compression of electric double layer and reduction in energy barrier for attachment. The parameter distributions of hydraulic conductivity (k), effective porosity (n_e), longitudinal dispersivity (α_L), vertical transverse dispersivity (α_{TV} /α_L) and horizontal transverse dispersivity (α_{TH} /α_L) estimated from the SiDNAmag and the salt tracer breakthrough curves were statistically similar. Our work contributes to the applicability of colloidal SiDNAmags for determining hydraulic parameters at different ionic strength conditions.

1. Introduction

Encapsulated DNA particles have recently attracted significant attention in tracer experiments for investigating subsurface flow, contaminant transport and porous media hydraulic properties characterization (Mikutis et al., 2018; Pang et al., 2020; Zhang et al., 2021; Kong et al., 2018; Kianfar et al., 2022; Chakraborty et al., 2022). In contrast to the conventional tracers (e.g. salt and fluorescent dyes), DNA particles have unique sequences, therefore, can ideally be produced in unlimited number of distinct particles and be used in multipoint injection experiments for aquifer characterization and contaminant transport tracking (Pang et al., 2020). In addition, DNA particles have low detection limit, high detection specificity in quantitative polymerase chain reaction (qPCR), no background noise interference due to uniqueness in nucleotide sequences (Liao et al., 2018). Encapsulated DNA particles have higher stability against environmental physico-chemical stressors (pH, UV radiation, enzymatic and microbial activity) (Sharma et al., 2012; Mikutis et al., 2018) as well.

Under unfavourable condition to colloid - collector attachment, colloidal attachment increased with increasing ionic strength (IS) for polystyrene spheres (Nocito-Gobel and Tobiason, 1996; Wu et al., 2020; Tufenkji and Elimelech, 2005; Tiraferri et al., 2011; Li et al., 2021; Xu et al., 2022) due to compression of electric double layer. Such compression led to weakened electrostatic repulsion between the colloid and collector grains and increased depth of secondary energy minimum (Xu et al., 2022; Wu et al., 2020; Bolster et al., 2001; Kermani et al., 2021). A fraction of heterogeneous collector surface contributing to colloid immobilization can induce a primary or a secondary energy

* Corresponding author.
E-mail address: s.chakraborty@uu.nl (S. Chakraborty).

https://doi.org/10.1016/j.advwatres.2023.104507
Received 8 February 2023; Received in revised form 20 July 2023; Accepted 25 July 2023
Available online 26 July 2023

minima interaction as well. Primary minima interaction and re-entrainment, while generally considered to be IS independent (Torkzaban and Bradford, 2016), may be influenced when the area of Zone Of electrostatic Influence (ZOI) is greater than the area of surface heterogeneity (Bradford et al., 2012) and colloids are deposited on rough patches (Torkzaban and Bradford, 2016). In contrast, Wang et al. (2011), observed an approximate 10-fold reduction in attachment efficiency of *E. coli* when IS increased from 10 to 100 mM. A decrease in *E. coli* zeta potential and subsequent increase in the repulsive energy barrier (DLVO) at higher IS hindered bacterial deposition. In addition to the ionic strength, phosphate ions reduced colloid attachment efficiency (α) and attachment rate (k_{att}), therefore, enhanced colloidal mobility (Chen et al., 2021; Liu et al., 2017, 2015; Wang et al., 2019; Zhang et al., 2018; Lin et al., 2021; Li and Schuster, 2014; Wang et al., 2011; Wang et al., 2020). The reduction in α and k_{att}, were attributed to the adsorption of phosphate onto the colloids and competitively on favourable deposition sites on collector grains leading to increased repulsive energy barrier and electrostatic repulsion.

One important implication of IS dependent colloidal release/deposition had been reported to alter the hydraulic conductivity (k) of porous media (Soma and Papadopoulos, 1995; Xinqiang et al., 2019; Won et al., 2018; Dikinya et al., 2008; Samari-Kermani et al., 2021; Torkzaban et al., 2015; Ochi and Vernoux, 1999; Ye et al., 2019). Xinqiang et al. (2019) attributed the reduction in k to "superficial" clogging due to higher colloid attachment at higher ISs (30 and 150 mM). Similarly, in column experiments with core samples, Torkzaban et al. (2015), attributed the reduction in the hydraulic conductivity to the hydrodynamic bridging of colloids at the pore constrictions. When the colloid to collector diameter ratio ranged between 0.01 to 0.25, at ionic strengths of 1 mM – 100 mM, Won et al., (2018) attributed reduction in k to straining due to higher detachment at lower ionic strength. Won and Burns, (2017) attributed the reduction of the k at lower ionic strength (1 mM $CaCl_2$) to straining due to aggregation or clustering of clay particles. Similarly, higher colloid release from collector grains, a function of lowered IS (1 mM), was reported to decrease 'k' due to pore clogging (Dikinya et al., 2008). In contrast, in 60 cm saturated sand (d_{50} = 375 μm) column experiments, at ionic strengths ranging between 0 and 13.68 mM, Mesticou et al. (2013), did not observe any reduction in the sand hydraulic conductivity. However, with longer experiment duration, the authors conclude that the pore clogging and therefore, permeability reduction would have occurred caused by the suspended colloids at the column inlet. In addition to permeability changes due to IS, colloid attachment onto the collector grains could affect the dispersivity estimation of colloids (Vasiliadou and Chrysikopoulos, 2011; Syngouna and Chrysikopoulos, 2011). Studies on the quantitative effect of IS on the effective porosity and dispersivity estimation are still limited. Since there is no general trend of permeability, effective porosity or dispersivity modification as a function of IS, and the modifications are influenced by critical colloid-collector ratio and critical deposition concentration (Bradford et al., 2002), a colloid and collector grain specific evaluation is required.

Stochastic methods are required for identifying simulation errors in hydraulic parameter estimations in deterministic models (Yan and Ji-Chun, 2005) and to represent parameter uncertainties (Ptak et al., 2004). Monte Carlo algorithm is a robust tool for uncertainty assessment of aquifer hydraulic parameters (Hoffmann et al., 2019; Fu and Gomez-Hernandez, 2009), spatial variability of hydraulic parameters (Herrick et al., 2002; Yan and Chun, 2005; Lapcevic et al., 1999; Chen et al., 2012), and to evaluate tracer specific parameter sensitivity (Hoffmann et al., 2019). Saley et al. (2016) successfully adopted Monte Carlo approach for reconstructing hydraulic conductivity distribution using heat tracer. Herrick et al. (2002) determined the correlation between hydraulic gradient, hydraulic conductivity and pore water velocity using Monte Carlo approach.

A number of studies have previously investigated groundwater flow, solute and contaminant transport, characterized hydraulic parameters of 3D laboratory models of saturated sand medium (Danquigny et al., 2004; Fadugba et al., 2018; Illman et al., 2012; Ojuri and Ola, 2010), or Karst aquifer systems (Mohammadi et al., 2021). A limited number of studies so far have used encapsulated DNA particles for aquifer hydraulic properties characterization (Mikutis et al., 2018; Kong et al., 2018). To our knowledge, we are the first to evaluate the use of SiDNAmag for estimating permeability, effective porosity, and longitudinal dispersivity (k, n_e and α_L, respectively) using a Monte Carlo approach under environmentally relevant and varying injection water quality parameters in a 3D system. The additional advantage of SiDNAmag over non-magnetic DNA particles is that in large scale experiments, the superparamagnetic property of SiDNAmags' imparts the advantage of rapid magnetic separation, therefore, no sample volume and up-concentration limitations (Sharma et al., 2021). The objectives of this study were to investigate the effect of IS perturbation of pore water by injection water on (1) transport of SiDNAmag microparticles in saturated porous media and, (2) probability distribution estimation of aquifer k, n_e and α_L parameters. We hypothesize that if the IS of SiDNAmag injection suspensions are varied between 1 mM, 5 mM and 20 mM of phosphate buffer, then the differences between the estimated probability distributions of k, n_e and α_L at different injection ISs would be statistically insignificant. Therefore, the aquifer parameter estimation would remain uninfluenced by varying extent of SiDNAmag deposition and release rates.

2. Materials and method

2.1. Silica-encapsulated ds-DNA superparamagnetic particles (SiDNAmag)

We obtained stock suspensions of (0.75 mg/ml ~10^{10} particles-ml^{-1}) of two uniquely sequenced SiDNAmags ($SiDNAmag_1$ and $SiDNAmag_2$) (Particle Engineering Research Centre, NTNU, Norway) in demineralized water. The diameter of $SiDNAmag_1$ and $SiDNAmag_2$ were 206.4 ± 85.6 nm and 183.9 ± 58.1 nm and zeta (ζ) potentials were −11 and −14mv in demineralized water, respectively.

2.2. SiDNAmag and sand

We suspended 50μL of the SiDNAmag stock suspensions in 5 ml of demineralized water. Then, we treated the 5 ml SiDNAmag suspension with 1μL of bleach to remove any free DNA present in the suspension. This was followed by washing the suspension twice by magnetic separation (BioRad, the Netherlands) of SiDNAmags to remove the bleach from the suspension. Finally, we prepared the injection suspension by resuspending the magnetically separated SiDNAmags in 1, 5, and 20 mM phosphate buffer solutions to a final concentration of ~ 10^6 particles/ml. The stability of the suspended particles in different injection waters were evaluated by means of ζ-potential using Smoluchowski's equation (dielectric constant $_{water}$ = 78.54) (Malvern Panalytical Zetasizer Nano-Zs ZEN 3600, the Netherlands), at a concentration of ~10^7 particles/ml. We checked the possibility of SiDNAmag aggregation within the experiment time interval by measuring hydrodynamic diameter (D_{hyd}) (Malvern Panalytical Zetasizer Nano-Zs ZEN 3600, the Netherlands), as a function of time (0, 60, 120 and 240 min), of particles suspended in tap water, 1, 5 and 20 mM phosphate buffer, in quiescent condition (Tang et al., 2021). We checked the ζ-potential of the quartz sand by dispersing 0.1 g of manually ground sand in 10 ml of tap water, 1 mM, 5 mM and 20 mM phosphate buffer.

2.3. Sand tank preparation and injection experiments

We homogeneously wet packed the 1.3 m (1.3 m x 0.7 m x 0.4 m) long sand tank with quartz sand fraction of 500–700 μm diameter (Sibelco, Belgium). The dimension of the sand tank was determined through pre-modelling of hypothetical solute transport experiments in

groundwater flow model, MODFLOW (Harbaugh, 2005), and solute transport module MT3DMS (Zheng and Wang, 1999). The dimension of 1.3 m x 0.7 m x 0.4 m was sufficient for performing multipoint and multilevel injection experiments with distinct breakthrough curves as outputs, and, for, parameter estimation.

The sand was wet packed with gradual height increment in order to minimize air entrapment and consolidation (Ojuri and Ola, 2010). Further, to achieve saturation, we flushed the sand tank for 10 – 12 h with tap water prior to the experiments. In order to inspect the uniform packing throughout the sand tank, we conducted multiple small scale (20 – 30 cm) salt tracer tests (data not shown) using the observation wells and compared the peak arrival time. In order to maintain constant hydraulic heads during the experiments, we pumped tap water at a rate of 511 ± 7.1 mL/min into the inflow chamber. We monitored the inflow and the outflow (~505 ± 7.3 mL/min) rates gravimetrically. The resulting hydraulic heads at the inflow chamber and the outflow chamber were 0.36 m and 0.32 m, respectively. The injection points, the sampling points and the screen depths are shown in Fig. 1. We injected 400 ml of salt (1.8 g/L) and 100 ml of SiDNAmag (~10^6 particles/ml) sequentially at injection rates of 400 ml / min and 100 ml/min, respectively. Further, we determined the concentration of the salt and the SiDNAmags as a function of time by measuring electric conductivity (WTW-Portable conductivity meter ProfiLine Cond 3310, Germany) and the DNA concentration using qPCR (Bio-Rad laboratories, USA), respectively, in samples collected at a 5 min interval. The sampling was done intermittently slow abstraction using plastic syringes in order to avoid the effect on the flow near the well. The protocol followed for qPCR had been detailed in Chakraborty et al. (2022). For representing, analysing and transport modelling of the salt breakthrough curves, we considered the datapoints above the background salt concentration by subtracting the background electric conductivity (EC_{BG}) from observed concentration (EC) and injection concentration (EC_0) using

$$\frac{EC}{EC_0} = \frac{EC - EC_{BG}}{EC_0 - EC_{BG}} \tag{1}$$

For simulation of the SiDNAmag breakthrough curves, we considered only the rising limbs, time to peak and the declining limbs. We did not consider the datapoints at the breakthrough tails since the concentrations were near the no template control (NTC) and similar to the scattered datapoints prior to the breakthrough. Therefore, we treated the breakthrough tail datapoints as uncertainty in sample analysis and did not include in the parameter estimation process (for k_{det}). For the breakthrough tails, we did not present the simulated breakthrough curves as well.

2.4. Breakthrough curve analysis and 3D modelling

We analysed the BTCs for both the salt tracer and the SiDNAmags in terms of time to peak (t_{peak}) and the maximum effluent concentration (C_{max}/C_0) for all the sampling locations. Then, we determined the k, n_e, and α_L parameter uncertainty, by subjecting the breakthrough curves to 3-dimensional convective-diffusive transport modelling, adopting a Monte-Carlo inverse approach, considering the first order kinetic non-equilibrium attachment and detachment processes primarily controlling the SiDNAmag transport through saturated porous media.

2.5. Groundwater, the salt and the SiDNAmag transport modelling

Encapsulated DNA particles and silica colloids' transport through saturated porous media were implicitly explained using classical convection-dispersion equation for solute transport with first order kinetic attachment – detachment process/term (Chakraborty et al., 2022). The partial differential equation used to simulate the (pore water flow equation not shown) convective-dispersive salt and SiDNAmag transport along with first order kinetic mass transfer from aqueous to solid phase was (Zheng and Wang, 1999)

$$n_e\frac{\partial C}{\partial t} + k_{att}n_eC - k_{det}\rho_bS = \frac{\partial}{\partial x_i}\left(n_eD_{ij}\frac{\partial C}{\partial x_j}\right) - \frac{\partial}{\partial x_i}(n_ev_iC) \tag{2}$$

Where C is the salt tracer or SiDNAmag concentration in the water, n_e is the effective porosity [-], D_{ij} is the hydrodynamic dispersion coefficient tensor [m^2/min], k_{att} is the first order attachment rate [1/min] and k_{det} is the first order detachment rate of the colloids [1/min], v_i is the pore water velocity [m/min] and represent the hydraulic conductivity (k) as $v_i = -(k / n_e) * (\delta_h/\delta_l)$, where v_i is the pore water velocity [m/min], k is the hydraulic conductivity [m/min], n_e is the effective porosity [-] and δ_h/δ_l is the hydraulic gradient [-]. S is the SiDNAmag concentration of attachment SiDNAmags [kg/kg], ρ_b is the bulk density of the sand [kg/m^3] and t is the time of transport [min]. In the SiDNAmag transport module, k_{att} is represented by β/n_e [1/min], where β is the mass transfer rate from water to the sand [1/min]. k_{det} is represented by $\beta/\rho_b k_d$ [1/min], where k_d is the distribution coefficient [m^3/kg] (Babakhani, 2019).

We considered straining not to be an important process in the SiDNAmag transport since the colloid to sand grain diameter ratio was 0.0003, which was well below the threshold of 0.003 (Bradford and Bettahar, 2006) and 0.004 (Johnson et al., 2010). Also, the salt and the SiDNAmag concentration in the injection suspension did not alter the viscosity and density of the injection water, therefore, we did not include density effect in the modelling process.

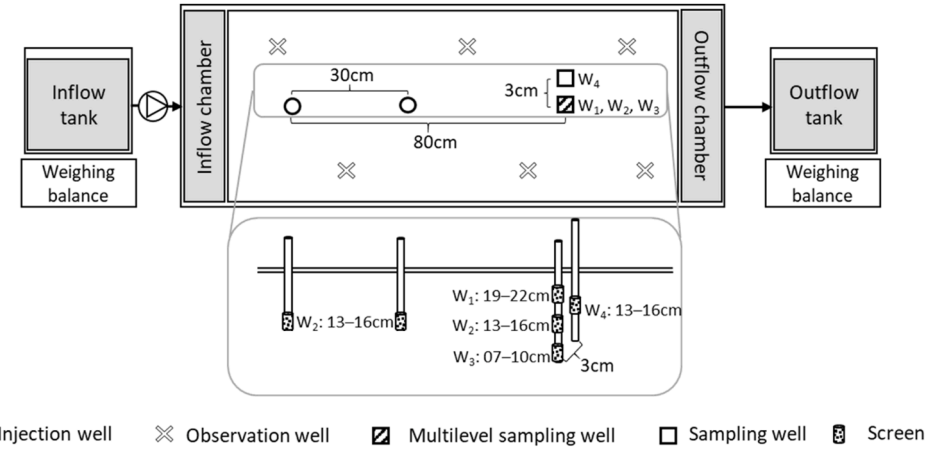

Fig. 1. Schematic experimental setup.

2.6. Monte Carlo simulation and parameter uncertainty analysis

We performed the simulations using a finite difference groundwater flow model, Modflow-2005 (Harbaugh, 2005) in conjunction with a solute transport module, MT3DMS (Zheng and Wang, 1999) in a python package, Flopy (Bakker et al., 2016). We spatially discretized the 1.3 m x 0.7 m x 0.36 m tank model into 12 layers of equal thickness, each layer thickness corresponding to the length of the injection or sampling screen. The first layer was assigned as unconfined and rest of the 11 layers as unconfined/confined. We temporally discretized the mass transport in three stress periods for stabilizing the hydraulic heads (50 min), injection period (1 min) and the sampling period (200 min). The

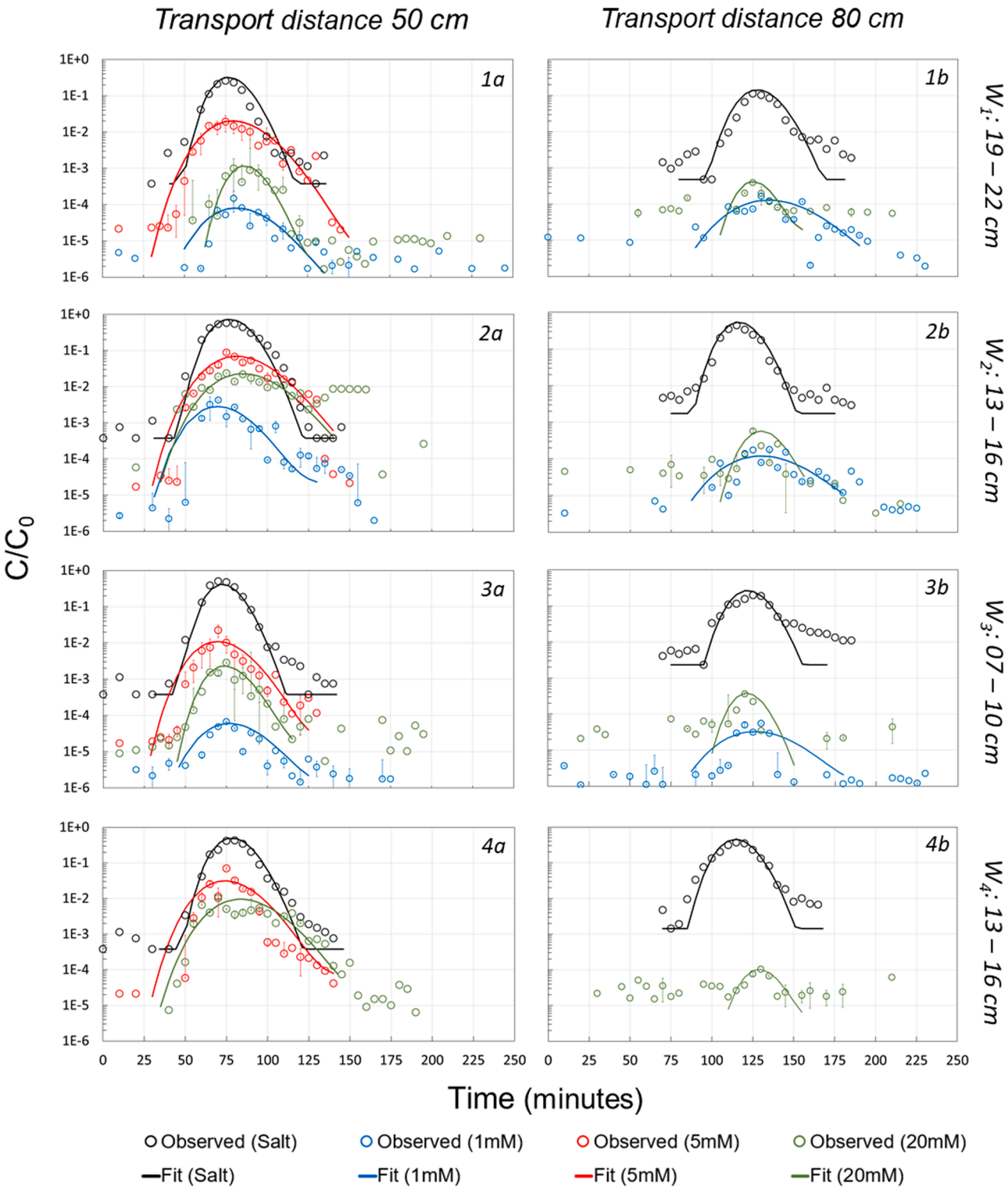

Fig. 2. BTCs of conservative and SiDNAmag at sampling location W_1 (above injection depth, central flow line); W_2 (at injection depth, central flow line); W_3 (below injection depth, central flow line), and W_4 (at injection depth, transverse horizontally perpendicular to central flow line); at 50 cm (left column) and 80 cm (right column) transport distance, respectively, for injection suspension of 1 mM, 5 mM and 20 mM PO_4 buffer. All reported depths were measured from the bottom of the tank. The BTCs include the relative SiDNAmag concentrations above no template control (NTC).

input ranges of k, ne and α_L, were 0.05 – 0.15 [m/min], 0.2 – 0.5 [-], and 10^{-8} – 10^{-1} [m], respectively. We estimated the input k and the n_e ranges as ±50% of the average k and n_e estimated from observed hydraulic heads and Darcy's law. The hydraulic heads and therefore, the hydraulic gradients were measured at the observation, injection and the sampling wells. Then we estimated the k by dividing the Darcy flux by the hydraulic gradients ($q = -k * i$), where q is the Darcy flux [m/min] and i is the hydraulic gradient [-]. We approximated the initial n_e by dividing q by average linear velocity (v) obtained from the initially conducted small scale salt tracer experiments. The input range for β was 0.001 – 0.1 [1/min] and the k_d was set to 1 [1/min]. The solute and SiDNAmag transport equation (Eq. (1)) was solved for 20,000 uniformly distributed random realization sets of k, n_e, α_L, and k_{att} for each of the ionic strength conditions. The goodness of fit of the parameter sets were evaluated based on minimized $RMSE_{log}$ combined for all sampling locations and transport distance. We did not emphasize on the coefficient of correlation (R^2) as an objective function since a higher R^2 could be achieved even when the BTC magnitudes are not matched (Ward et al., 2017). Based on the minimized objective function, we considered the top 1% as the best parameter value sets. Then, we evaluated the normality of the parameter distributions through Kolmogorov – Smirnov test and Quantile – Quantile plot (QQ plot). Since not all the distributions followed a normal distribution, we assessed the statistical differences of the parameter distributions using the distribution non-specific Mann Whitney U test (significance level = 0.05). The simulated breakthrough curves (Fig. 2) are presented based on the median values obtained for each parameter.

3. Results

3.1. SiDNAmag and sand characterization

The ζ potential of the SiDNAmags decreased with increasing IS of phosphate buffer (Table 1). The ζ potentials of the $SiDNAmag_1$ (injected for 0.5 m transport length) were −47.7, −44.1, and −39.9 mV, while dispersed in 1 mM, 5 mM and 20 mM phosphate buffer, respectively. The ζ potentials of the $SiDNAmag_2$ (injected for 0.8 m transport length) were −43, −40.7, and −38.5 mV, while dispersed in 1 mM, 5 mM and 20 mM phosphate buffer, respectively. In tap water, the ζ potentials of both the SiDNAmags were ~ - 22 mV. The ζ potentials indicated acceptable stability (−20 mV < ζ < +20 mV) in all water types. The ζ potentials of sand were −26.3, −37.7, −50.7, and −49.3 mV in tap water, 1, 5, and 20 mM phosphate buffer, respectively. The negative ζ potentials of both the sand and the SiDNAmag under all ionic strength conditions indicated that colloid transport was conducted under unfavourable condition for colloid attachment onto the sand grains (repulsive double layer interaction). D_{hyd} of the $SiDNAmag_1$ were 442.3, 644.6, and 652.3 nm, while dispersed in 1 mM, 5 mM and 20 mM phosphate buffer, respectively. D_{hyd} of the $SiDNAmag_2$ were 516.9, 660.5, and 655.8 nm, while dispersed in 1 mM, 5 mM and 20 mM phosphate buffer, respectively. The D_{hyd} of the SiDNAmags did not change significantly throughout the experiment interval (240 min), indicating that particle aggregation was unlikely to occur (Table 1).

3.2. Salt and SiDNAmag breakthrough curves

All the sampling locations combined, the time to peaks (t_{peaks}) for salt tracer at 0.5 m and 0.8 m transport distances ranged between 75 – 80 min and 120 – 125 min, respectively. The t_{peaks} of the SiDNAmag dispersed in 1 mM suspension for 0.5 m and 0.8 m transport distances were 75 – 80 min and 130 – 135 min respectively. SiDNAmags suspended in 5 mM suspension reached the maximum effluent concentration at 70 – 75 min for 0.5 m transport distance. The t_{peaks} of the SiDNAmags suspended in 20 mM injection suspension were 75 – 80 min and 120 – 130 min, for 0.5 m and 0.8 m transport distances, respectively. Though the t_{peak} of SiDNAmags, under all ionic strength conditions, were similar to the salt tracer, the maximum effluent concentrations (C_{max}/C_0) of SiDNAmags were 1 – 4 log units lower than the salt tracer. At 0.5 m transport distance, the C_{max}/C_0 of the salt tracer, SiDNAmags in 1 mM, 5 mM and 20 mM ranged between 0.26 – 0.57, 0.000067 – 0.0042, 0.019 – 0.088, and 0.001 – 0.023 [-], respectively. At 0.8 m transport distance, C_{max}/C_0 for the salt, SiDNAmags in 1 mM, and 20 mM were 0.11 – 0.43, 0.000018 – 0.00015, and 0.0001 – 0.0024 [-], respectively. In comparison with 50 cm transport distance, the lower $C_{max}/C_{0,\ and}$ fewer datapoints near the centre of SiDNAmag mass indicated that under our experimental conditions, the transport of SiDNAmag was limited. The maximum C_{max}/C_0 of salt and SiDNAmag concentration were observed at W_2 since W_2 was installed at the injection depth. The SiDNAmag to salt ratio of area under the breakthrough curves were in the order of magnitude of 10^{-3} - 10^{-4}, 10^{-1} – 10^{-2}, and 10^{-2} – 10^{-3}, for 1 mM, 5 mM, and 20 mM injection suspension, respectively. The 5th – 95th percentile ranges of the parameters estimated from the salt and the SiDNAmag BTCs are summarised in Table 2.

3.3. Estimation of parameter uncertainty

The median k values for the salt tracers and SiDNAmags dispersed in 1 mM, 5 mM, and 20 mM phosphate buffer injection water were 0.072, 0.077 – 0.078, 0.074, and 0.08 [m/min], respectively. The statistical test showed that the parameter distributions (5th – 95th percentile) were not statistically significantly different from each other (Fig. 3). The median n_e for the salt tracers, SiDNAmags dispersed in 1 mM, 5 mM, and 20 mM phosphate buffer injection water were 0.36, 0.34 – 0.35, 0.36, and 0.34 [-], respectively. The n_e of SiDNAmags, like k, increased slightly as

Table 1
Differently DNA-tagged injected particles ($SiDNAmag_1$ and $SiDNAmag_2$) characterization and experimental conditions. The zeta (ζ) potentials were measured at particle concentrations ~4E+5 and 6E+5 particles ml^{-1}, for $SiDNAmag_1$ and $SiDNAmag_2$, respectively.

	Time (min)	Injection suspension								Sand		
		Salt		$SiDNAmag_1$			$SiDNAmag_2$					
		NaCl	Uranine	1mM	5mM	20mM	1mM	5mM	20mM	1mM	5mM	20mM
EC [µS/cm]		3120	517	183	860	2930	183	860	2930	–		
pH [-]		6.8		7.1								
ζ ± Stdev [-mV]		–	–	−47.7 ± 3.8	−44.1 ± 3.8	−39.9 ± 2.2	−43.0 ± 4.3	−40.7 ± 2.9	−38.5 ± 3.0	−37.7 ± 19.3	−50.7 ± 11.5	−49.3 ± 13.1
D_{hyd} ± Stdev [nm]	0	–	–	442.3 ± 39.1	644.6 ± 101	652.6 ± 125	516.9 ± 91.9	660.5 ± 108	655.8 ± 84.6	–		
	60	–	–	591.2 ± 98	691.4 ± 41	729.3 ± 118	523 ± 56.1	656.6 ± 87.4	608.22 ± 101			
	120	–	–	478.6 ± 58	678.5 ± 59	698.4 ± 99	577.5 ± 77	698.1 ± 104	688.65 ± 88.2			
	240	–	–	505.2 ± 102	623.5 ± 121	702.5 ± 79	528.7 ± 117	602.7 ± 97.1	622 ± 98.7			

† injected at 0.5 m transport length, ‡ injected at 0.8 m transport length.

Table 2
Breakthrough curve characteristics (C_{max}/C_0 and t_{peak}) at different sampling locations and the hydraulic conductivity (K), effective porosity (n_e), longitudinal dispersivity (α_L), horizontal transverse (α_{TH} / α_L), and vertical transverse (α_{TV} / α_L) dispersivity estimated from the salt tracer and the SiDNAmag.

		Transport distance [m]	Sampling location	C_{max}/C_0 [-]	t_{peak} [min]	K [m/min]	n_e [-]	α_L [m]	K_{att} [1/min]
Salt tracer		0.5	W_1	0.26	75	0.074 (0.074 – 0.082)[†]	0.36 (0.31 – 0.38)	9.16e-4 (3.2e-5 – 9.34e-4)	–
			W_2	0.57	75				
			W_3	0.5	75				
			W_4	0.42	80				
		0.8	W_1	0.11	125				
			W_2	0.43	120				
			W_3	0.39	120				
			W_4	0.19	125				
SiDNAmag	1mM	0.5	W_1	1.48e-4	80	0.078 (0.07 – 0.08)	0.35 (0.31 – 0.38)	2.6e-4 (8.8e-5 – 4.72e-4)	0.061 (0.055 – 0.068)
			W_2	4.2e-3	70				
			W_3	6.77e-5	75				
			W_4	–	–				
		0.8	W_1	1.64e-4	130	0.077 (0.07 – 0.1)	0.34 (0.33 – 0.37)	5.5e-4 (9.9e-5 – 7.84e-4)	0.05 (0.041 – 0.058)
			W_2	1.78e-5	135				
			W_3	5.47e-5	130				
			W_4	–	–				
	5mM	0.5	W_1	1.9e-2	75	0.074 (0.07 – 0.084)	0.36 (0.32 – 0.37)	1e-4 (6.2e-5 – 7.87e-4)	0.019 (0.013 – 0.022)
			W_2	8.8e-2	75				
			W_3	2.2e-2	70				
			W_4	7e-2	75				
		0.8	W_1	–	–	–	–	–	–
			W_2	–	–				
			W_3	–	–				
			W_4	–	–				
	20mM	0.5	W_1	9.9e-4	80	0.08 (0.075 – 0.082)	0.34 (0.33 – 0.37)	9.7e-4 (8e-5 – 6.9e-4)	0.035 (0.031 – 0.042)
			W_2	2.4e-2	75				
			W_3	2.8e-3	75				
			W_4	1e-2	70				
		0.8	W_1	3.94e-4	125	0.08 (0.076 – 0.081)	0.34 (0.31 – 0.38)	1.8e-4 (3.2e-5 – 9.6e-4)	0.054 (0.051 – 0.063)
			W_2	5.77e-4	120				
			W_3	3.61e-4	120				
			W_4	1.04e-4	130				

[†] 5th – 95th percentile of the parameter uncertainty
- Not analysed.

compared to the salt tracer, however, the n_e distributions were not statistically different from each other. The median α_L for the salt tracers, SiDNAmags dispersed in 1 mM, 5 mM, and 20 mM phosphate buffer injection water were 9.16×10^{-4}, $2.6 \times 10^{-4} - 5.5 \times 10^{-4}$, 1×10^{-4}, and 1.8×10^{-4} - 9.7×10^{-4} [m], respectively. The parameter distribution of SiDNAmags within the 5th – 95th percentile for all the ionic strength condition, were statistically not different than those of the salt tracer. The attachment rate (K_{att}) of the SiDNAmags dispersed in 1 mM, 5 mM and 20 mM, onto the sand grains were 0.05 – 0.061, 0.019, and 0.035 – 0.054 [1/min], respectively, which was reflected on the order of maximum effluent concentration as a function of ionic strength of the injection water.

4. Discussion

The average velocity of salt ($6.4 \times 10^{-3} - 6.7 \times 10^{-3}$ m/min) and the SiDNAmag (6×10^{-3} - 7×10^{-3}) at both 50 cm and 80 cm transport distances were similar to each other irrespective of the ionic strength of the injection water. The similar time of maximum concentration (t_{peak}) of the salt and SiDNAmags dispersed in the injection water of 1 mM, 5 mM, and 20 mM ionic strengths indicated that size exclusion or velocity enhancement did not occur. Our observation was similar to Wu et al. (2020), where within a range of 1 mM – 20 mM NaCl suspension, no early arrival or velocity enhancement was observed for 100 nm polystyrene nanoparticles transporting through dessert soil (86% sand). In a 15 cm column, with similar colloid and collector grain size, Chakraborty et al. (2022) observed similar time of maximum effluent concentration indicating absence of velocity enhancement. In fine sand (180 – 250 μm) and at a linear velocity of 0.009 m/min, Harter et al. (2000) did not observe earlier breakthrough or velocity enhancement for 4500 – 5500 μm Cryptosporidium Parvum oocysts, though at larger grain sizes the velocity enhancement was apparent. Absence of size exclusion of velocity enhancement of colloids in our experiments was possibly due to the collector size being 3 orders of magnitude higher, and the average pore throat size being ~2 orders of magnitude higher as compared to the SiDNAmags. This ratio was much higher than the threshold of 1.5, observed by Sirivithayapakorn and Keller, (2003). In contrast to our observation, earlier arrival and velocity enhancement, with similar colloid size and grain size, as used in this study, had been reported by Mikutis et al. (2018), which could be due to the difference in the linear velocity used. There are other studies (Nocito-Gobel and Tobiason, 1996; Grolimund et al., 1998; Higgo et al., 1993; Keller et al., 2004) which reported the occurrences of size exclusion and velocity enhancement at varying colloid size, collector size and average linear velocities.

Considering the maximum SiDNAmag concentration in the effluent, the SiDNAmags showed least attachment (k_{att}) and highest mobility while dispersed in 5 mM phosphate buffer, followed by 20 mM and 1 mM phosphate buffer injection suspension. The slightly higher attachment rate, and therefore, the 0.5 – 1 log unit reduction in the maximum effluent concentration for SiDNAmags in 20 mM phosphate suspension as compared to 5 mM injection suspension agreed with most of the studies on the effect of ionic strength on the colloid transport (Xu et al., 2022; Wu et al., 2020; Bolster et al., 2001). Nocito-Gobel and Tobiason (1996), observed least attachment and maximum mobility of latex particles at an NaCl concentration of 0.1 and 1 mM as compared to 5 mM and 10 mM. Similar decrease in the attachment efficiency was reported by Bolster et al. (2001) for bacterial transport upon reduction of ionic strength from 100 mM to 10 mM of KCl. Reduction in attachment efficiency and attachment rates with decreasing ionic strength were attributed to the compression of electric double layer leading to reduced depth of secondary energy minimum and weakened electrostatic

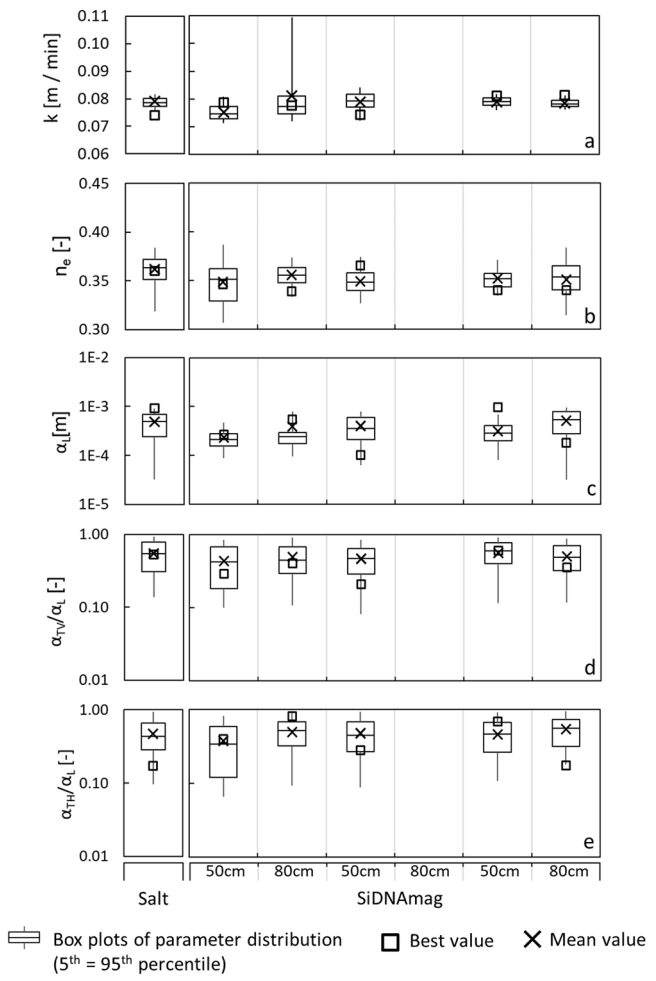

Fig. 3. Estimated value ranges of (a) hydraulic conductivity, (b) effective porosity, (c) longitudinal dispersivity for salt tracer (NaCl, fluorescein) and SiDNAmag dispersed in phosphate buffer of varying ISs (1 mM, 5 mM and 20 mM).

repulsion between the colloids and the collector grains (Xu et al., 2022; Wu et al., 2020; Bolster et al., 2001). Therefore, we attributed the increase in attachment with increasing ionic strength of the injection suspension to the compression of electric double layer resulting in weakened electrostatic repulsion. However, a decrease in SiDNAmag attachment in 5 mM injection water as compared to 1 mM was in contradiction with the widely reported observations (Nocito-Gobel and Tobiason, 1996; Wu et al., 2020, Tufenkji and Elimelech, 2005). This contrast with our result can be explained by the competitive attachment of phosphate ions on the favourable attachment sites onto the collector grains. As reported by Chen et al. (2021), addition of 0.5 mM phosphate suspension in saturated columns increased the maximum effluent concentration by ~3% and ~17% in clean and goethite coated sand, respectively. When phosphate concentration increased form 0.1 mM to 1 mM, Wang et al. (2011), reported an increase in *E. coli* recovery from ~45% to ~77% at an NaCl concentration of 10 mM. Silica colloid transport increased from ~11% to ~48% in a quartz sand column in the presence of 0.5 mM phosphate due to a reduction in zeta potential of the colloids (Liu et al., 2017). Such reduction in attachment and enhancement in colloid transport in the presence of phosphate had been attributed to the adsorption of phosphate onto the colloids and collector grains leading to an increased colloid – colloid and colloid – collector repulsion (Chen et al., 2015; Liu et al., 2017). This increase in the repulsion increased primary energy barrier for attachment (Wang et al., 2019; Zhang et al., 2018; Li and Schuster, 2014).

Our results indicated that the hydraulic parameter (k, n_e, and α_L) distributions estimated from the salt tracers and the SiDNAmags were statistically similar and therefore, were independent to the ionic strengths used in this study. In this regard, our results were similar to the Mesticou et al. (2013), where reduction in *k* did not occur at ionic strengths ranged between 0 and 13.68 mM, with similar sand grain size and silica colloids of 1.3 – 22 μm diameter. Similarly, Soma and Papadopoulos (1995), observed only a small (7%) reduction in k at lower ionic strengths (0.5 and 5 mM). The *k* reduction had been attributed to the pore constriction clogging due to straining (Ochi and Vernouz, 1999; Torkzaban et al., 2015), aggregation of colloids (Won et al., 2020; Xinqiang et al., 2019; Dikinya et al., 2008), and colloid aggregation on the collector surface (Ye et al., 2019). Since the colloid aggregation increases with increasing ionic strength, therefore pore clogging and the reduction in *k* were reported to increase with increasing ionic strength as well (Xinqiang et al., 2019; Ye et al., 2019; Won et al., 2020). However, the highly negative ζ – potentials and the constant D_{hyd} of the SiDNAmags suspended in all ionic strengths throughout the experiment interval implied that SiDNAmag aggregation was unlikely to occur. In addition, the colloid and collector ratio (0.0003 [-]) in our experiments was an order of magnitude lower than the threshold of 0.004 (Johnson et al., 2010) or 0.003 (Bradford and Bettahar, 2006) for straining. Overall, at the experimental conditions and the range of ionic strengths used in our work, the 3D transport behaviour of the salt tracers and the SiDNAmags dispersed 1 mM, 5 mM and 20 mM phosphate buffer suspension were statistically not different.

However, under our experimental condition, we identified a limitation of using the SiDNAmag. The particles showed limited travel at 80 cm transport distance, reflected on the low effluent concentration. Therefore, only a small number of datapoints could be modelled to estimate the conductivity and the effective porosity. The low SiDNAmag injection concentration was possibly limiting our findings and should be considered in the future work.

5. Conclusion

- Under all ionic strength conditions, the recovery of SiDNAmags were 1 – 4 log units reduced as compared to the salt tracers due to colloid attachment onto the collector grains. We observed the maximum SiDNAmag transport under 5 mM ionic strength injection suspension followed by 20 mM and 1 mM injection water ionic strength.
- We conclude that lower attachment rate of SiDNAmags at 5 mM injection suspension as compared to 1 mM injection water was due to the competitive adsorption of negatively charged phosphate ions on the favourable attachment sites of collector grains. At comparatively higher ionic strength, i.e. 20 mM injection suspension, the attachment rate increased due to the compression of electric double layer resulting in lower energy barrier.
- Comparing the salt tracers and colloids (SiDNAmags) transport breakthrough curves, we found that at all ionic strength of injection water, the estimated hydraulic parameter distributions (hydraulic conductivity, effective porosity, and longitudinal dispersivity) were not statistically significantly different. Therefore, we can accept our null hypothesis that the ionic strengths do not have effect on the hydraulic parameter distributions
- We did not observe size exclusion or velocity enhancement of the SiDNAmags resulting in earlier breakthrough of the SiDNAmags. This was possibly due to the three orders of magnitude higher grain size diameter as compared to the SiDNAmags, therefore, high pore size to SiDNAmag size ratio.
- The implication of this study lies in that, under homogeneous, saturated, and unconsolidated sand and within the ionic strength range used in this work, the SiDNAmags have similar three dimensional transport properties as the salt and can be applied for determining the hydraulic parameters of a 3D system

CRediT authorship contribution statement

Swagatam Chakraborty: Conceptualization, Methodology, Software, Investigation, Data curation, Writing – original draft, Writing – review & editing. **Rayan Elhaj:** Investigation, Data curation. **Jan Willem Foppen:** Conceptualization, Methodology, Resources, Writing – review & editing, Supervision, Funding acquisition. **Jack Schijven:** Conceptualization, Methodology, Resources, Writing – review & editing, Supervision, Funding acquisition.

Declaration of Competing Interest

The authors declare that they have no known competing financial interests or personal relationships that could have appeared to influence the work reported in this paper.

Data availability

Data will be made available on request.

Acknowledgment

This research had been funded by the Dutch Research Council (NWO), TTW Grant 14514. We would like to thank Dr. Sulalit Bandyopadhyay, Department of Chemical Engineering, Faculty of Natural Sciences, NTNU, Norway for the kind contribution with SiDNAmag particles. We would like extend our gratitude to thank Dr. Thom Bogaard, Department of Civil Engineering and Geosciences, TU-Delft, the Netherlands, for his contribution and support with experimental setup preparation and modelling. We would like to thank Hortus Botanicus, TU-Delft, the Netherlands; and IHE-Delft, the Netherlands for the laboratory work support.

References

Babakhani, P., 2019. The impact of nanoparticle aggregation on their size exclusion during transport in porous media: one-and three-dimensional modelling investigations. Sci. Rep. 9 (1), 1–12. https://doi.org/10.1038/s41598-019-50493-6.

Bakker, M., Post, V., Langevin, C.D., Hughes, J.D., White, J.T., Starn, J.J., Fienen, M.N., 2016. Scripting MODFLOW model development using Python and FloPy. Groundwater 54 (5), 733–739. https://doi.org/10.1111/gwat.12413.

Bolster, C.H., Mills, A.L., Hornberger, G.M., Herman, J.S., 2001. Effect of surface coatings, grain size, and ionic strength on the maximum attainable coverage of bacteria on sand surfaces. J. Contam. Hydrol. 50 (3–4), 287–305. https://doi.org/10.1016/S0169-7722(01)00106-1.

Bradford, S.A., Bettahar, M., 2006. Concentration dependent transport of colloids in saturated porous media. J. Contam. Hydrol. 82 (1–2), 99–117. https://doi.org/10.1016/j.jconhyd.2005.09.006.

Bradford, S.A., Torkzaban, S., Kim, H., Simunek, J., 2012. Modeling colloid and microorganism transport and release with transients in solution ionic strength. Water Resour. Res. 48 (9) https://doi.org/10.1029/2012WR012468.

Bradford, S.A., Yates, S.R., Bettahar, M., Simunek, J., 2002. Physical factors affecting the transport and fate of colloids in saturated porous media. Water Resour. Res. 38 (12), 63. https://doi.org/10.1029/2002WR001340.

Chakraborty, S., Foppen, J.W., Schijven, J.F., 2022. Effect of concentration of silica encapsulated ds-DNA colloidal microparticles on their transport through saturated porous media. Colloids Surf. A 651, 129625. https://doi.org/10.1016/j.colsurfa.2022.129625.

Chen, J., Chen, W., Lu, T., Song, Y., Zhang, H., Wang, M., Lu, M., 2021. Effects of phosphate on the transport of graphene oxide nanoparticles in saturated clean and iron oxide-coated sand columns. J. Environ. Sci. 103, 80–92. https://doi.org/10.1016/j.jes.2020.10.011.

Chen, M., Xu, N., Cao, X., Zhou, K., Chen, Z., Wang, Y., Liu, C., 2015. Facilitated transport of anatase titanium dioxides nanoparticles in the presence of phosphate in saturated sands. J. Colloid Interface Sci. 451, 134–143. https://doi.org/10.1016/j.jcis.2015.04.010.

Chen, X., Zhang, Y.F., Xue, X., Zhang, Z., Wei, L., 2012. Estimation of baseflow recession constants and effective hydraulic parameters in the karst basins of southwest China. Hydrol. Res. 43 (1–2), 102–112. https://doi.org/10.2166/nh.2011.136.

Danquigny, C., Ackerer, P., Carlier, J.P., 2004. Laboratory tracer tests on three-dimensional reconstructed heterogeneous porous media. J. Hydrol. 294 (1–3), 196–212. https://doi.org/10.1016/j.jhydrol.2004.02.008.

Dikinya, O., Hinz, C., Aylmore, G., 2008. Decrease in hydraulic conductivity and particle release associated with self-filtration in saturated soil columns. Geoderma 146 (1–2), 192–200. https://doi.org/10.1016/j.geoderma.2008.05.014.

Fadugba, O.G., Ola, S.A., Ojuri, O.O., 2018. Remediation of Petroleum Hydrocarbons in a tropical Sand Tank Model, 1. Springer International Publishing, pp. 185–195. https://doi.org/10.1007/978-3-319-61612-4_15.

Fu, J., Gómez-Hernández, J.J., 2009. Uncertainty assessment and data worth in groundwater flow and mass transport modeling using a blocking Markov chain Monte Carlo method. J. Hydrol. 364 (3–4), 328–341. https://doi.org/10.1016/j.jhydrol.2008.11.014.

Grolimund, D., Elimelech, M., Borkovec, M., Barmettler, K., Kretzschmar, R., Sticher, H., 1998. Transport of in situ mobilized colloidal particles in packed soil columns. Environ. Sci. Technol. 32 (22), 3562–3569. https://doi.org/10.1021/es980356z.

Harbaugh, A.W., 2005. MODFLOW-2005, the U.S. geological survey modular ground-water model – the ground-water flow processU.S. Geological Survey Techniques and Methods 6-A16, 6.

Harter, T., Wagner, S., Atwill, E.R., 2000. Colloid transport and filtration of Cryptosporidium parvum in sandy soils and aquifer sediments. Environ. Sci. Technol. 34 (1), 62–70. https://doi.org/10.1021/es990132w.

Herrick, M.G., Benson, D.A., Meerschaert, M.M., McCall, K.R., 2002. Hydraulic conductivity, velocity, and the order of the fractional dispersion derivative in a highly heterogeneous system. Water Resour. Res. 38 (11), 9. https://doi.org/10.1029/2001WR000914. -1.

Higgo, J.J.W., Williams, G.M., Harrison, I., Warwick, P., Gardiner, M.P., Longworth, G., 1993. Colloid transport in a glacial sand aquifer. laboratory and field studies. In: Colloids in the Aquatic Environment, pp. 179–200. https://doi.org/10.1016/B978-1-85861-038-2.50016-4.

Hoffmann, R., Dassargues, A., Goderniaux, P., Hermans, T., 2019. Heterogeneity and prior uncertainty investigation using a joint heat and solute tracer experiment in alluvial sediments. Front. Earth Sci. 7, 108. https://doi.org/10.3389/feart.2019.00108.

Illman, W.A., Berg, S.J., Yeh, T.C.J., 2012. Comparison of approaches for predicting solute transport: sandbox experiments. Groundwater 50 (3), 421–431. https://doi.org/10.1111/j.1745-6584.2011.00859.x.

Johnson, W.P., Pazmino, E., Ma, H., 2010. Direct observations of colloid retention in granular media in the presence of energy barriers, and implications for inferred mechanisms from indirect observations. Water Res. 44 (4), 1158–1169. https://doi.org/10.1016/j.watres.2009.12.014.

Keller, A.A., Sirivithayapakorn, S., Chrysikopoulos, C.V., 2004. Early breakthrough of colloids and bacteriophage MS2 in a water-saturated sand column. Water Resour. Res. 40 (8) https://doi.org/10.1029/2003WR002676.

Kianfar, B., Tian, J., Rozemeijer, J., van der Zaan, B., Bogaard, T.A., Foppen, J.W., 2022. Transport characteristics of DNA-tagged silica colloids as a colloidal tracer in saturated sand columns; role of solution chemistry, flow velocity, and sand grain size. J. Contam. Hydrol. 246, 103954 https://doi.org/10.1016/j.jconhyd.2022.103954.

Kong, X.Z., Deuber, C.A., Kittilä, A., Somogyvári, M., Mikutis, G., Bayer, P., Saar, M.O., 2018. Tomographic reservoir imaging with DNA-labeled silica nanotracers: the first field validation. Environ. Sci. Technol. 52 (23), 13681–13689. https://doi.org/10.1021/acs.est.8b04367.

Lapcevic, P.A., Novakowski, K.S., Sudicky, E.A., 1999. The interpretation of a tracer experiment conducted in a single fracture under conditions of natural groundwater flow. Water Resour. Res. 35 (8), 2301–2312. https://doi.org/10.1029/1999WR900143.

Li, L., Schuster, M., 2014. Influence of phosphate and solution pH on the mobility of ZnO nanoparticles in saturated sand. Sci. Total Environ. 472, 971–978. https://doi.org/10.1016/j.scitotenv.2013.11.057.

Li, M., Zhang, X., Yi, K., He, L., Han, P., Tong, M., 2021. Transport and deposition of microplastic particles in saturated porous media: co-effects of clay particles and natural organic matter. Environ. Pollut. 287, 117585 https://doi.org/10.1016/j.envpol.2021.117585.

Liao, R., Yang, P., Wu, W., Luo, D., Yang, D., 2018. A DNA tracer system for hydrological environment investigations. Environ. Sci. Technol. 52 (4), 1695–1703. https://doi.org/10.1021/acs.est.7b02928.

Lin, D., Bradford, S., Hu, L., MC Lo, I., 2021. Impact of phosphate adsorption on the mobility of PANI-supported nano zero-valent iron. Vadose Zone J. 20 (2), e20091. https://doi.org/10.1002/vzj2.20091.

Liu, C., Xu, N., Feng, G., Zhou, D., Cheng, X., Li, Z., 2017. Hydrochars and phosphate enhancing the transport of nanoparticle silica in saturated sands. Chemosphere 189, 213–223. https://doi.org/10.1016/j.chemosphere.2017.09.066.

Mesticou, Z., Kacem, M., Dubujet, P.H., 2013. Influence of the ionic strength on the deposit phenomenon and transport dynamic of microparticles through saturated porous medium. COUPLED V:. In: Proceedings of the V International Conference on Computational Methods for Coupled Problems in Science and Engineering. CIMNE, pp. 1168–1178 http://hdl.handle.net/2117/192762.

Mikutis, G., Deuber, C.A., Schmid, L., Kittilä, A., Lobsiger, N., Puddu, M., Stark, W.J., 2018. Silica-encapsulated DNA-based tracers for aquifer characterization. Environ. Sci. Technol. 52 (21), 12142–12152. https://doi.org/10.1021/acs.est.8b03285.

Mohammadi, Z., Illman, W.A., Field, M., 2021. Review of laboratory scale models of karst aquifers: approaches, similitude, and requirements. Groundwater 59 (2), 163–174. https://doi.org/10.1111/2Fgwat.13052.

Nocito-Gobel, J., Tobiason, J.E., 1996. Effects of ionic strength on colloid deposition and release. Colloids Surf. A 107, 223–231. https://doi.org/10.1016/0927-7757(95)03340-8.

Ochi, J., Vernoux, J.F., 1999. A two-dimensional network model to simulate permeability decrease under hydrodynamic effect of particle release and capture. Transp. Porous Media 37 (3), 303–325. https://doi.org/10.1023/A:1006690700000.
Ojuri, O.O., Ola, S.A., 2010. Estimation of contaminant transport parameters for a tropical sand in a sand tank model. Int. J. Environ. Sci. Technol. 7, 385–394. https://doi.org/10.1007/BF03326148.
Pang, L., Abeysekera, G., Hanning, K., Premaratne, A., Robson, B., Abraham, P., Billington, C., 2020. Water tracking in surface water, groundwater and soils using free and alginate-chitosan encapsulated synthetic DNA tracers. Water Res. 184, 116192 https://doi.org/10.1016/j.watres.2020.116192.
Ptak, T., Piepenbrink, M., Martac, E., 2004. Tracer tests for the investigation of heterogeneous porous media and stochastic modelling of flow and transport—A review of some recent developments. J. Hydrol. 294 (1–3), 122–163. https://doi.org/10.1016/j.jhydrol.2004.01.020.
Saley, A.D., Jardani, A., Ahmed, A.S., Antoine, R., Dupont, J.P., 2016. Hamiltonian Monte Carlo algorithm for the characterization of hydraulic conductivity from the heat tracing data. Adv. Water Res. 97, 120–129. https://doi.org/10.1016/j.advwatres.2016.09.004.
Samari-Kermani, M., Jafari, S., Rahnama, M., Raoof, A., 2021. Ionic strength and zeta potential effects on colloid transport and retention processes. Colloid Interface Sci. Commun. 42, 100389 https://doi.org/10.1016/j.colcom.2021.100389.
Sharma, A.N., Luo, D., Walter, M.T., 2012. Hydrological tracers using nanobiotechnology: proof of concept. Environ. Sci. Technol. 46 (16), 8928–8936. https://doi.org/10.1021/es301561q.
Sharma, A., Foppen, J.W., Banerjee, A., Sawssen, S., Bachhar, N., Peddis, D., Bandyopadhyay, S., 2021. Magnetic nanoparticles to unique DNA tracers: effect of functionalization on Physico-chemical properties. Nanoscale Res. Lett. 16 (1), 1–16. https://doi.org/10.1186/s11671-021-03483-5.
Sirivithayapakorn, S., Keller, A., 2003. Transport of colloids in saturated porous media: a pore-scale observation of the size exclusion effect and colloid acceleration. Water Resour. Res. 39 (4) https://doi.org/10.1029/2002WR001583.
Soma, J., Papadopoulos, K.D., 1995. Flow of dilute, sub-micron emulsions in granular porous media: effects of pH and ionic strength. Colloids Surf. A 101 (1), 51–61. https://doi.org/10.1016/0927-7757(95)03200-W.
Syngouna, V.I., Chrysikopoulos, C.V., 2011. Transport of biocolloids in water saturated columns packed with sand: effect of grain size and pore water velocity. J. Contam. Hydrol. 126 (3–4), 301–314. https://doi.org/10.1016/j.jconhyd.2011.09.007.
Tang, Y., Foppen, J.W., Bogaard, T.A., 2021. Transport of silica encapsulated DNA microparticles in controlled instantaneous injection open channel experiments. J. Contam. Hydrol. 242, 103880 https://doi.org/10.1016/j.jconhyd.2021.103880.
Tiraferri, A., Tosco, T., Sethi, R., 2011. Transport and retention of microparticles in packed sand columns at low and intermediate ionic strengths: experiments and mathematical modeling. Environ. Earth Sci. 63, 847–859. https://doi.org/10.1007/s12665-010-0755-4.
Torkzaban, S., Bradford, S.A., 2016. Critical role of surface roughness on colloid retention and release in porous media. Water Res. 88, 274–284. https://doi.org/10.1016/j.watres.2015.10.022.
Torkzaban, S., Bradford, S.A., Vanderzalm, J.L., Patterson, B.M., Harris, B., Prommer, H., 2015. Colloid release and clogging in porous media: effects of solution ionic strength and flow velocity. J. Contam. Hydrol. 181, 161–171. https://doi.org/10.1016/j.jconhyd.2015.06.005.
Tufenkji, N., Elimelech, M., 2005. Breakdown of colloid filtration theory: role of the secondary energy minimum and surface charge heterogeneities. Langmuir 21 (3), 841–852. https://doi.org/10.1021/la048102g.
Vasiliadou, I.A., Chrysikopoulos, C.V., 2011. Cotransport of Pseudomonas putida and kaolinite particles through water-saturated columns packed with glass beads. Water Resour. Res. 47 (2) https://doi.org/10.1029/2010WR009560.
Wang, D., Paradelo, M., Bradford, S.A., Peijnenburg, W.J., Chu, L., Zhou, D., 2011a. Facilitated transport of Cu with hydroxyapatite nanoparticles in saturated sand: effects of solution ionic strength and composition. Water Res. 45 (18), 5905–5915. https://doi.org/10.1016/j.watres.2011.08.041.
Wang, L., Xu, S., Li, J., 2011b. Effects of phosphate on the transport of Escherichia coli O157: H7 in saturated quartz sand. Environ. Sci. Technol. 45 (22), 9566–9573. https://doi.org/10.1021/es201132s.
Wang, S., Li, D., Zhang, M., Chen, M., Xu, N., Yang, L., Chen, J., 2020. Competition between fulvic acid and phosphate-mediated surface properties and transport of titanium dioxide nanoparticles in sand porous media. J. Soils Sediments 20, 3681–3687. https://doi.org/10.1007/s11368-020-02699-9.
Wang, Z., Shen, C., Du, Y., Zhang, Y., Li, B., 2019. Influence of phosphate on deposition and detachment of TiO_2 nanoparticles in soil. Front. Environ. Sci. Eng. 13, 1–11. https://doi.org/10.1007/s11783-019-1163-y.
Ward, A.S., Kelleher, C.A., Mason, S.J., Wagener, T., McIntyre, N., McGlynn, B., Payn, R. A., 2017. A software tool to assess uncertainty in transient-storage model parameters using Monte Carlo simulations. Freshw. Sci. 36 (1), 195–217. https://doi.org/10.1086/690444.
Won, J., Choo, H., Burns, S.E., 2020. Impact of solution chemistry on deposition and breakthrough behaviors of kaolinite in silica sand. J. Geotech. Geoenviron. Eng. 146 (1), 04019123 https://doi.org/10.1061/(ASCE)GT.1943-5606.0002199.
Wu, X., Lyu, X., Li, Z., Gao, B., Zeng, X., Wu, J., Sun, Y., 2020. Transport of polystyrene nanoplastics in natural soils: effect of soil properties, ionic strength and cation type. Sci. Total Environ. 707, 136065 https://doi.org/10.1016/j.scitotenv.2019.136065.
Xinqiang, D., Yalin, S., Xueyan, Y., Ran, L., 2019. Colloid clogging of saturated porous media under varying ionic strength and roughness during managed aquifer recharge. J. Water Reuse Desalin. 9 (3), 225–231. https://doi.org/10.2166/wrd.2019.041.
Xu, L., Liang, Y., Liao, C., Xie, T., Zhang, H., Liu, X., Wang, D., 2022. Cotransport of micro-and nano-plastics with chlortetracycline hydrochloride in saturated porous media: effects of physicochemical heterogeneities and ionic strength. Water Res. 209, 117886 https://doi.org/10.1016/j.watres.2021.117886.
Yan, C.H.E.N., Ji-chun, W.U., 2005. Effect of the spatial variability of hydraulic conductivity in aquifer on the numerical simulation of groundwater. Adv. Water Sci. 16 (4), 482–487.
Ye, X., Cui, R., Du, X., Ma, S., Zhao, J., Lu, Y., Wan, Y., 2019. Mechanism of suspended kaolinite particle clogging in porous media during managed aquifer recharge. Groundwater 57 (5), 764–771. https://doi.org/10.1111/gwat.12872.
Zhang, W., Li, S., Wang, S., Lei, L., Yu, X., Ma, T., 2018. Transport of Escherichia coli phage through saturated porous media considering managed aquifer recharge. Environ. Sci. Pollut. Res. 25, 6497–6513. https://doi.org/10.1007/s11356-017-0876-3.
Zhang, Y., Hartung, M.B., Hawkins, A.J., Dekas, A.E., Li, K., Horne, R.N., 2021. DNA tracer transport through porous media—The effect of DNA length and adsorption. Water Resour. Res. 57 (2), 2020WR028382 https://doi.org/10.1029/2020WR028382.
Zheng, C., Wang, P.P., 1999. MT3DMS: a modular three-dimensional multispecies transport model for simulation of advection, dispersion, and chemical reactions of contaminants. In: groundwater systems; documentation and user's guide. Contract Report SERDP-99-1. U.S. Army Engineer Research and Development Center, Vicksburg, Mississippi.. http://hdl.handle.net/11681/4734